51st AIAA Aerospace Sciences Meeting including the New Horizons Forum and Aerospace Exposition
07 - 10 January 2013, Grapevine (Dallas/Ft. Worth Region), Texas

AIAA 2013-0326

Modeling of Jet Noise Sources and their Diffraction with Uniform Flow

Dimitri Papamoschou* and Salvador Mayoral †

University of California, Irvine, Irvine, CA, 92697, USA

A methodology is presented for treating the propagation of elementary jet noise sources in the presence of a uniform mean flow. The sources include wavepacket and point sources, and the propagation includes the diffraction around solid boundaries. The governing equations are reduced to the canonical wave equation through established transformations. The impact of the transformations on the wavepacket and point sources is discussed, with attention on the distinction between sources of pressure and sources of volume. The coupling of the transformations with the boundary element method, for the prediction of diffraction, is outlined. The impact of uniform flow on the emission of an acoustic monopole produces a complicated pressure field with different near- and and far-field scaling laws. The principal effect of flight speed on the wavepacket emission is to shift the range of radiating axial wavenumbers, resulting in attenuation and re-direction of the acoustic emission. For both the wavepacket and monopole, the flight Mach number causes a compaction of the acoustic field downstream of the source, a trend that benefits the shielding of those sources.

Nomenclature

a_∞	=	freestream speed of sound
A	=	wavepacket amplitude function
f	=	cyclic frequency
G	=	Green's function
k	=	acoustic wavenumber $= \omega/a_\infty$
k_x	=	axial wavenumber
k_r	=	radial wavenumber
M_∞	=	freestream Mach number
M_c	=	convective Mach number
$R, R^*, \mathcal{R}$	=	source-observer distances
p	=	pressure
r	=	radial distance in polar coordinate system
Sr	=	Strouhal number
t	=	time
$\mathbf{u}$	=	velocity vector
U_∞	=	freestream velocity
$\mathbf{x} = (x, y, z)$	=	position vector
α	=	instability wavenumber
κ	=	modified acoustic wavenumber
θ	=	polar angle relative to jet axis
ψ	=	azimuth angle
ϕ	=	acoustic velocity potential
ρ_∞	=	freestream density
ω	=	angular frequency

*Professor, Department of Mechanical and Aerospace Engineering, Fellow AIAA
†Graduate Student Researcher, Department of Mechanical Aerospace Engineering, Member AIAA

Modifiers

$\widehat{(\ )}$	=	axial Fourier transform
$\widetilde{(\ )}$	=	transformed domain

I. Introduction

Prediction of propulsion-airframe integration noise requires physical models for the noise sources in conjunction with efficient propagation tools. The turbulent mixing noise of the engine exhaust is particularly challenging to model in a way that is physically meaningful yet simple enough to enable the development of design tools. Recently, the wavepacket model for the jet noise source has shown some promise in this regard.[1] The wavepacket, in combination with a weak monopole, captures the far-field directivity of the jet noise and provides diffraction predictions that are in reasonable agreement with experiments. The process involves the development of a parametric model, calibration of the model parameters by matching the experimental statistics of the isolated jet, and application of the model to the diffraction problem using a suitable propagation scheme, such as the boundary element method (BEM)[2] or the fast scattering code (FSC).[3]

The aforementioned diffraction predictions had been conducted for static jets. Aircraft noise is inherently based on forward flight, so it is important to include the Mach number effects in the modeling and propagation of the noise sources. The first-order approximation is to treat the flow field as uniform, which enables transformations that reduce the problem to a static form for all subsonic Mach numbers. Alternative approaches treat propagation in a potential flow field, but are limited to low Mach number.[4]

This report outlines the methodology for treating wavepacket and point sources with uniform flow for the purpose of source parameterization and eventual prediction of scattering. The methodology involves transformations that reduce the convective wave equation to the canonical wave equation. Even though these transformations are established, there are subtleties that unless understood could lead to erroneous approaches. For this reason, the report starts from the fundamentals and provides a methodical treatment of the transformations in the time and frequency domains. For consistency, all the transformed parameters are indicated by the $\widetilde{(\ )}$ notation.

II. Theoretical Background

This section provides a review of sound propagation in uniform flow and the basis of the boundary element method.

A. Time Domain Analysis

1. Convective wave equation

Consider the acoustic propagation in a medium with a uniform mean velocity U_∞ in the x-direction and constant mean speed of sound a_∞ (Fig. 1). The velocity field is

$$\mathbf{u}(\mathbf{x},t) \ = \ U_\infty \mathbf{i} \ + \ \mathbf{u}'(\mathbf{x},t)$$

where $\mathbf{i}$ is the unit vector in the axial direction. The propagation of an acoustic pressure disturbance p' is governed by the convective wave equation

$$\frac{1}{a_\infty^2}\frac{\partial^2 p'}{\partial t^2} + 2\frac{M_\infty}{a_\infty}\frac{\partial^2 p'}{\partial x \partial t} - \left[(1-M_\infty^2)\frac{\partial^2 p'}{\partial x^2} + \frac{\partial^2 p'}{\partial y^2} + \frac{\partial^2 p'}{\partial z^2}\right] = 0 \tag{1}$$

The acoustic potential ϕ and the density perturbation ρ' also satisfy the above equation. Comparing with the canonical wave equation we note two differences: the mixed-derivative term $\partial^2/\partial x \partial t$ and the "Prandtl-Glauert" factor $1-M_\infty^2$ multiplying the $\partial^2/\partial x^2$ term. The momentum equation relates pressure and acoustic potential as follows:

$$p' \ = \ -\rho_\infty \frac{\overline{D}\phi}{Dt} \ = \ \frac{\partial \phi}{\partial t} + U_\infty \frac{\partial \phi}{\partial x} \tag{2}$$

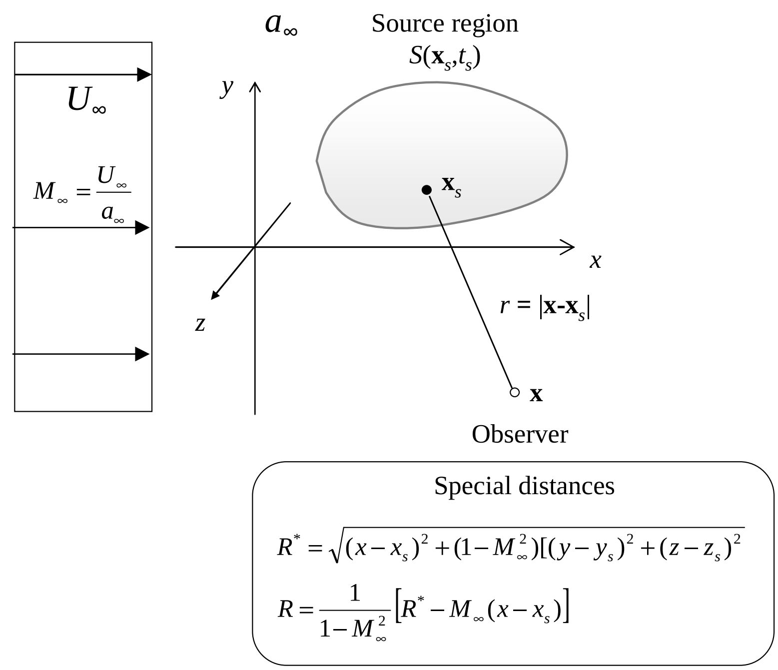

Figure 1. Acoustics with uniform flow.

2. Transformation to the canonical form

The Lorentz-type transformations

$$\begin{aligned} \tilde{t} &= \sqrt{1-M_\infty^2}\; t + \frac{1}{\sqrt{1-M_\infty^2}} \frac{M_\infty}{a_\infty}\; x \\ \widetilde{x} &= \frac{x}{\sqrt{1-M_\infty^2}} \end{aligned} \tag{3}$$

reduce the convective wave equation to the canonical form

$$\frac{\partial^2 p'}{\partial \tilde{t}^2} - a_\infty^2 \nabla_{\widetilde{x}}^2\, p' \;=\; 0 \tag{4}$$

with

$$\nabla_{\widetilde{x}} \;=\; \left(\frac{\partial}{\partial \widetilde{x}}, \frac{\partial}{\partial y}, \frac{\partial}{\partial z} \right)$$

This enables the use of tools developed for the classical wave equation. The problem is solved in the transformed domain, then converted to the original domain by reversing the transformations. Note that first-order relations like Eq. 2 do not transform into their static counterparts.

3. Solutions using free-space Green's function

In the transformed domain, the free-space Green's function satisfies

$$\frac{\partial^2 \widetilde{G}}{\partial \tilde{t}^2} - a_\infty^2 \nabla_{\widetilde{x}}^2 \widetilde{G} \;=\; \delta(\widetilde{\mathbf{x}} - \widetilde{\mathbf{x}}_s)\delta(\tilde{t} - \tilde{t}_s) \tag{5}$$

and its solution is

$$\widetilde{G}(\widetilde{\mathbf{x}}, \tilde{t} | \widetilde{\mathbf{x}}_s, \tilde{t}_s) \;=\; \frac{1}{4\pi |\widetilde{\mathbf{x}} - \widetilde{\mathbf{x}}_s|} \delta(\tilde{t} - \tilde{t}_s - |\widetilde{\mathbf{x}} - \widetilde{\mathbf{x}}_s| / a_\infty) \tag{6}$$

Expressed in the original coordinates, the Green's function becomes

$$G(\mathbf{x},t|\mathbf{x}_s,t_s) = \frac{1}{4\pi R^*}\delta(t-t_s-R/a_\infty) \tag{7}$$

$$R = \frac{1}{1-M_\infty^2}[R^* - M_\infty(x-x_s)] \tag{8}$$

$$R^* = \sqrt{(x-x_s)^2+(1-M_\infty^2)[(y-y_s)^2+(z-z_s)^2]} \tag{9}$$

This form of the Green's function was first derived by Blokhintsev.[5] It has since been used by a variety of investigations, such as Ref. 6.

Knowledge of the free-space Green's functions with uniform flow allows construction of the solution for an arbitrary source in a 3D unbounded domain.

$$p'(\mathbf{x},t) = \int_{\mathcal{V}_s} \frac{S_p(\mathbf{x}_s, t-R/a_\infty)}{4\pi R^*} d^3\mathbf{x}_s \tag{10}$$

$$\phi(\mathbf{x},t) = \int_{\mathcal{V}_s} \frac{S_\phi(\mathbf{x}_s, t-R/a_\infty)}{4\pi R^*} d^3\mathbf{x}_s \tag{11}$$

with R and R^* as defined in Eqs. 8 and 9, respectively. Here S_p and S_ϕ are sources for the pressure and velocity potential, respectively. This distinction is important because the convection effects act differently on each type of source.

B. Frequency Domain

1. Governing equation

On applying the substitutions

$$\begin{aligned} p'(\mathbf{x},t) &\rightarrow p(\mathbf{x})e^{-i\omega t} \\ \phi(\mathbf{x},t) &\rightarrow \phi(\mathbf{x})e^{-i\omega t} \end{aligned} \tag{12}$$

the convective wave equation (Eq. 1) assumes the harmonic form

$$k^2 p - 2ikM_\infty \frac{\partial p}{\partial x} - \left[(1-M_\infty^2)\frac{\partial^2 p}{\partial x^2} + \frac{\partial^2 p}{\partial y^2} + \frac{\partial^2 p}{\partial z^2}\right] = 0 \tag{13}$$

The relation between pressure and acoustic potential, Eq. 2, becomes

$$p(\mathbf{x}) = -\rho_\infty\left(-i\omega + U_\infty\frac{\partial}{\partial x}\right)\phi(\mathbf{x}) = \rho_\infty a_\infty\left(ik - M_\infty\frac{\partial}{\partial x}\right)\phi(\mathbf{x}) \tag{14}$$

2. Transformation to the canonical form

To reduce the problem to the ordinary Helmholtz equation the transformations of Eq. 3 are used. The new variable $\widetilde{x}$ reduces the terms inside the brackets of Eq. 13 to the Laplacian in the coordinate system $(\widetilde{x}, y, z)$. The time transformation can be written as

$$t = \frac{\tilde{t}}{\sqrt{1-M_\infty^2}} - \frac{M_\infty}{a_\infty}\frac{\widetilde{x}}{\sqrt{1-M_\infty^2}}$$

and eliminates the second term on the left-hand side of Eq. 13. The full expression for p' becomes

$$p(\mathbf{x})e^{-i\omega t} = p(\mathbf{x})\exp\left(-i\frac{\omega}{\sqrt{1-M_\infty^2}}\tilde{t}\right)\exp\left(i\frac{\omega}{a_\infty}\frac{M_\infty}{\sqrt{1-M_\infty^2}}\widetilde{x}\right)$$

This means that we are working with a new frequency $\tilde{\omega} = \omega/\sqrt{1-M_\infty^2}$ and thus a new wavenumber $\widetilde{k} = k/\sqrt{1-M_\infty^2}$. In addition, the dependent variable is no longer p but the transformed variable

$$\widetilde{p} = pe^{i\kappa\widetilde{x}} \tag{15}$$

with $\kappa = kM_\infty/\sqrt{1-M_\infty^2}$. Equation 13 reduces to the ordinary Helmholtz equation in the transformed domain:

$$\nabla^2_{\widetilde{x}}\widetilde{p} \ + \ \widetilde{k}^2\widetilde{p} \ = \ 0 \tag{16}$$

In summary the variable and coordinate transformations are as follows:

$$\begin{aligned}
(x,y,z) \ &\rightarrow \ (\widetilde{x},y,z) \ , && \widetilde{x} \ = \ \frac{x}{\sqrt{1-M_\infty^2}} \\
\omega \ &\rightarrow \ \widetilde{\omega}, && \widetilde{\omega} \ = \ \frac{\omega}{\sqrt{1-M_\infty^2}} \\
k \ &\rightarrow \ \widetilde{k}, && \widetilde{k} \ = \ \frac{k}{\sqrt{1-M_\infty^2}} \\
\widetilde{p} \ &= \ pe^{i\kappa\widetilde{x}}, && \kappa = k\frac{M_\infty}{\sqrt{1-M_\infty^2}}
\end{aligned} \tag{17}$$

These transformations can be found in several past works, including the paper by Wu and Lee,[7] with the difference that they assumed a harmonic convention $\exp(+i\omega t)$. Working directly in the frequency domain one may miss that the variable and frequency transformations in Eq. 17 originate from the simple t and x transformations of Eq. 3.

3. Green's function solutions

The Green's function in the transformed domain satisfies

$$\nabla^2_{\widetilde{x}}\widetilde{G} \ + \ \widetilde{k}^2\widetilde{G} \ = \ -\delta(\widetilde{\mathbf{x}}-\widetilde{\mathbf{x}}_s) \tag{18}$$

whose solution is

$$\widetilde{G}(\widetilde{\mathbf{x}}|\widetilde{\mathbf{x}}_s) \ = \ \frac{1}{4\pi|\widetilde{\mathbf{x}}-\widetilde{\mathbf{x}}_s|}\exp(i\widetilde{k}|\widetilde{\mathbf{x}}-\widetilde{\mathbf{x}}_s|) \tag{19}$$

Obviously it has the same form as the Green's function for the static case. This enables the use of numerical methods based on the static free-space Green's function, such as the Boundary Element Method (BEM), to compute scattering problems in the transformed domain.

The Green's function may also be expressed in the original domain as

$$G(\mathbf{x}|\mathbf{x}_s) \ = \ \frac{e^{ikR}}{4\pi R^*} \tag{20}$$

with R and R^* defined in Eqs. 8 and 9. Therefore, the general solution for the harmonic problem is

$$\begin{aligned}
p(\mathbf{x}) \ &= \ \int_{\mathcal{V}_s} S_p(\mathbf{x}_s) \ \frac{e^{ikR}}{4\pi R^*} \ d^3\mathbf{x}_s \\
\phi(\mathbf{x}) \ &= \ \int_{\mathcal{V}_s} S_\phi(\mathbf{x}_s) \ \frac{e^{ikR}}{4\pi R^*} \ d^3\mathbf{x}_s \\
R = & \ \ \frac{1}{1-M_\infty^2}[R^* - M_\infty(x-x_s)] \\
R^* = & \ \ \sqrt{(x-x_s)^2+(1-M_\infty^2)[(y-y_s)^2+(z-z_s)^2]}
\end{aligned} \tag{21}$$

The distinction between sources of pressure (S_p) and sources of acoustic potential (S_ϕ) is again crucial as will be discussed in the next section. The solution form of Eq. 21 is useful for solving 3D free-space problems, but is not applicable to scattering problems using the standard BEM. To use the BEM, the computation needs to be done in the transformed domain.

4. Boundary Element Method

Boundary integral formulations are central to solving acoustic scattering and radiation problems.[2] The general problem setup is depicted in Fig. 3. Below is a brief review of the boundary element method for

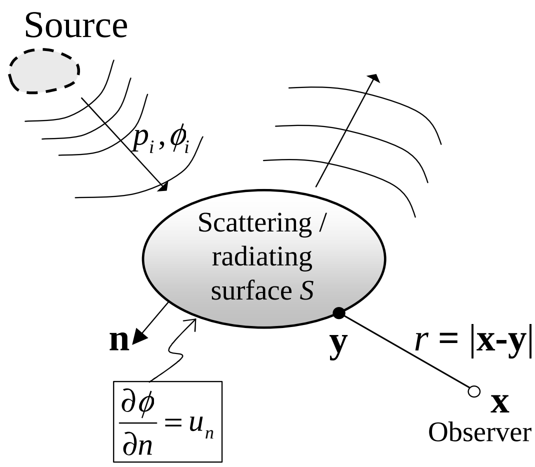

Figure 2. Acoustic scattering/radiation problem.

the canonical Helmholtz equation. Flow effects can be introduced by applying the BEM in the transformed domain.

The BEM has exactly the same form for all the acoustic scalar variables, although surface boundary conditions may be different for each variable. The BEM for the acoustic potential is

$$c(\mathbf{x})\phi(\mathbf{x}) \;=\; \int_S \left[G(\mathbf{x}|\mathbf{y}) \frac{\partial \phi(\mathbf{y})}{\partial n} - \frac{\partial G(\mathbf{x}|\mathbf{y})}{\partial n} \phi(\mathbf{y}) \right] d^2\mathbf{y} \;+ \phi_i(\mathbf{x}) \tag{22}$$

and the BEM for the acoustic pressure is

$$c(\mathbf{x})p(\mathbf{x}) \;=\; \int_S \left[G(\mathbf{x}|\mathbf{y}) \frac{\partial p(\mathbf{y})}{\partial n} - \frac{\partial G(\mathbf{x}|\mathbf{y})}{\partial n} p(\mathbf{y}) \right] d^2\mathbf{y} \;+ p_i(\mathbf{x}) \tag{23}$$

In the above equations, G is the Green's function; $c(\mathbf{x})$ takes the values 1 in the exterior, 1/2 on the surface (assuming the surface is smooth), and 0 in the interior of the body; and subscript i denotes the incident field. The variable or its normal derivative are prescribed on the surface (for example, p or $\partial p/\partial n$).

The normal velocity on the surface is

$$u_n \;=\; \mathbf{u} \cdot \mathbf{n} \;=\; \nabla \phi \cdot \mathbf{n} \;=\; \frac{\partial \phi}{\partial n} \tag{24}$$

Recalling the relation between pressure and acoustic potential in the static environment, Eq. 25, the normal derivative of the pressure is

$$\frac{\partial p}{\partial n} \;=\; i\omega\rho_\infty \frac{\partial \phi}{\partial n} \;=\; i\omega\rho_\infty u_n \tag{25}$$

For a rigid body, $u_n = 0$ so the normal derivatives of pressure and potential both vanish on the surface. So for problems of scattering by rigid bodies, the BIEs for pressure and acoustic potential will give identical results, within a constant.

III. Acoustic Monopole

A. Definition

The monopole is a volume source/sink visualized as a uniformly-pulsating sphere with radius ϵ much smaller than the acoustic wavelength $\lambda = a_\infty/f$, where f is the cyclic frequency. It is important to realize that the monopole, as traditionally defined, is a source of *volume*. Thus the velocity potential is the natural variable for the monopole. The monopole is not directly a source of pressure. The pressure is determined through the conservation equations once the solution for ϕ is obtained. Accordingly, the monopole source is

$$S_\phi(\mathbf{x}_s, t_s) \;= q(t_s)\delta(\mathbf{x}_s) \tag{26}$$

Applying the general solution of Eq. 7,

$$\phi(\mathbf{x},t) \;=\; -\frac{q(t-R/a_\infty)}{4\pi R^*} \tag{27}$$

with R and R^* defined by Eqs. 8 and 9. The solution for the pressure perturbation is

$$p'(\mathbf{x},t) \;=\; -\rho_\infty \frac{\overline{D}\phi}{Dt} \;=\; \rho_\infty \left(\frac{\partial}{\partial t} + U_\infty \frac{\partial}{\partial x}\right) \frac{q(t-R/a_\infty)}{4\pi R^*} \tag{28}$$

and results in a fairly complex expression.

For the harmonic problem $q(t) = Q\exp(-i\omega t)$,

$$\phi(\mathbf{x}) \;=\; Q\frac{e^{ikR}}{4\pi R^*} \tag{29}$$

and

$$p(\mathbf{x}) \;=\; \frac{\rho_\infty a_\infty Q}{4\pi}\left(-ik + M_\infty \frac{\partial}{\partial x}\right)\frac{e^{ikR}}{R^*} \tag{30}$$

After some straight-forward differentiations, the pressure field becomes

$$p(\mathbf{x}) \;=\; -Q\rho_\infty a_\infty \frac{e^{ikR}}{4\pi R^*}\left[ik\frac{1 - M_\infty \frac{x}{R^*}}{1 - M_\infty^2} + M_\infty \frac{x}{{R^*}^2}\right] \tag{31}$$

The pressure field thus becomes significantly more complicated than in the static case. Inside the square brackets, the first term depends on wavenumber and the second term is independent of wavenumber and decays with the square of the transformed distance. The second term disappears in the far field but it could be dominant in the near field, particularly at low wavenumber and high Mach number.

It is instructive to examine the amplitudes of the acoustic potential and the pressure. For the acoustic potential,

$$|\phi|(\mathbf{x}) \;= \frac{Q}{4\pi R^*} \tag{32}$$

We note that the magnitude of ϕ is independent of frequency (wavenumber). Recalling the definition of R^* from Eq. 9, the ϕ amplitude is affected by the Prandtl-Glauert transformation of the y and z coordinates. As the Mach number increases, there is a transverse stretching of the ϕ amplitude, so the disturbance penetrates more in the y and z directions. The amplitude of the pressure field is

$$|p|(\mathbf{x},k) \;= Q\rho_\infty a_\infty \frac{1}{4\pi R^*}\sqrt{k^2\left(\frac{1 - M_\infty \frac{x}{R^*}}{1 - M_\infty^2}\right)^2 + M_\infty^2 \frac{x^2}{{R^*}^4}} \tag{33}$$

In the far field, the second term inside the square root becomes negligible:

$$|p|(\mathbf{x},k) \;\approx Q\rho_\infty a_\infty \frac{k}{4\pi R^*}\frac{|1 - M_\infty \frac{x}{R^*}|}{1 - M_\infty^2} \tag{34}$$

For low Mach number ($M_\infty^2 << 1$), this further simplifies to

$$|p|(\mathbf{x},k) \;\approx Q\rho_\infty a_\infty \frac{k}{4\pi \mathcal{R}}\left|1 - M_\infty \frac{x}{R^*}\right| \tag{35}$$

where $\mathcal{R}$ is the physical distance between observer and monopole. Recognizing the terms outside the absolute value as the amplitude of the monopole in a static environment,

$$|p|(\mathbf{x},k) \;\approx |p_0|(\mathbf{x},k)\left|1 - M_\infty \frac{x}{r}\right| \tag{36}$$

where subscript 0 denotes the static case. It is evident from Eqs. 33-36 that the free stream causes an *upstream* amplification of the acoustic field. This effect was noted by Taylor[4] in his analysis of acoustic propagation in a moving medium.

The effect of the free stream on the acoustic field of the monopole is illustrated in Fig. 3. The monopole is situated at the origin $(0, 0, 0)$ and the Mach number takes the values $M_\infty = 0$, and 0.6. Figure 3 plots isocontours of the real part and the magnitude of the acoustic potential ϕ and pressure p. The contours of the real part of ϕ show the expected downstream convection of the wavefronts. As noted earlier, the magnitude of ϕ distorts into an oval-shaped distribution penetrating further into the transverse direction. The distortion is minimal at low Mach number. The complexity of the pressure field is evident by the contours of its real part. Notable are the downstream convection of the wavefronts and the amplification upstream of the monopole. The upstream amplification is further evident by the pressure magnitude contours; it is caused by the collapse of the wavefronts ahead of the monopole with increasing Mach number.

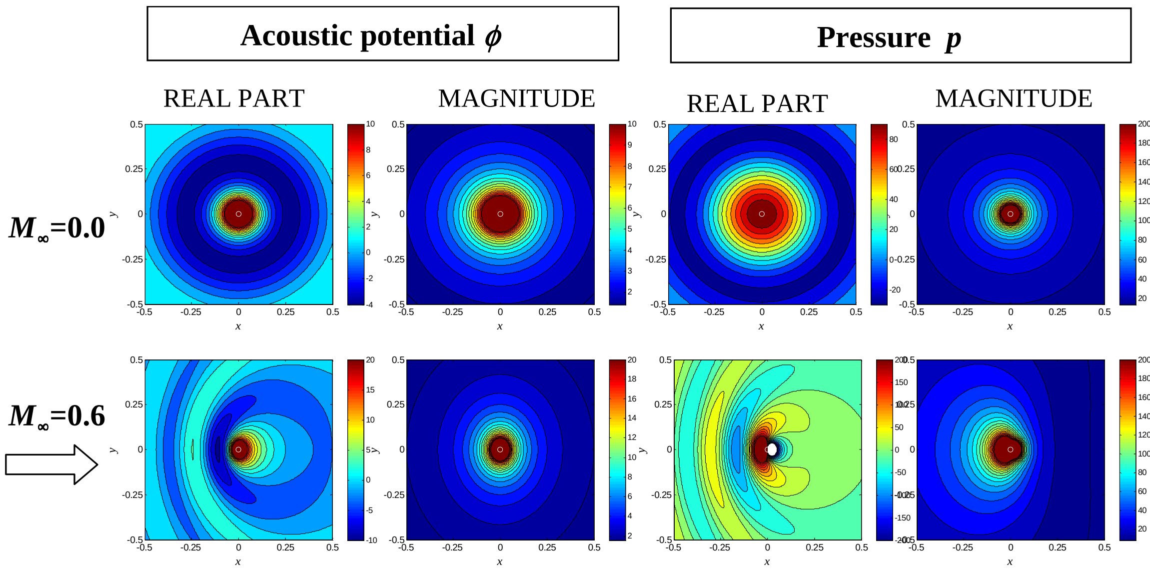

Figure 3. Acoustic fields for a monopole with $\rho_\infty a_\infty Q$=1 and $k = 10$.

B. Ramification on Selection of Green's Functions

Comparing the acoustic potential field of the monopole, Eq. 29, with the Green's function Eq. 20, we note that they are identical within a constant. On the other hand, the pressure field given by Eq. 31 is fundamentally different from the Green's function. This means that, for uniform flow, the Green's function represents the acoustic potential field of a monopole but does not represent its pressure field. To put it in a different way, the statement

$$S_p(\mathbf{x}_s, t_s) \ = q(t_s)\delta(\mathbf{x}_s)$$

does *not* represent a monopole in uniform flow. It represents a pressure point source (PPS) which does not have a physical basis. The distinction between the monopole and the PPS disappears at $M_\infty = 0$. With $M_\infty > 0$, however, their fields are different. When working in the transformed domain, the proper variable for the monopole is the acoustic potential. On the other hand, one may choose to work with the PPS as a fictitious source for the purpose of source parameterization, to be discussed in Section V. It is obvious that the pressure field for the PPS has the same form as the acoustic-potential field for the monopole, that is,

$$p(\mathbf{x}) \ = \ Q\frac{e^{ikR}}{4\pi R^*} \tag{37}$$

where Q now is the strength of the PPS and has no direct connection to volume injection.

IV. Wavepacket

A. Wavepacket as a Model for the Jet Noise Source

At its most general interpretation, the wavepacket model is an application of Kirchhoff's integral theorem.[8] The wavepacket model builds on the foundational works by Tam and Burton,[9] Crighton and Huerre,[10] Avital et al.[11] and Morris.[12] There is increasing experimental evidence that the peak noise radiation is caused by an instability-wave mechanism, as evidenced by a number of near-field experiments, for example the works of Reba et al.[13] Following the analysis by Morris,[12] we consider a cylindrical surface surrounding a turbulent jet (Fig. 4). The radius r_0 of the surface is sufficiently close to the jet to sense both the radiating and non-radiating (hydrodynamic) components of the turbulent pressure fluctuations. On the wavepacket surface $r = r_0$ we prescribe a pressure disturbance $p_0(x)e^{in\psi}$, or an acoustic potential $\phi_0(x)e^{in\psi}$, where n is the helical mode and ψ is the azimuthal angle.

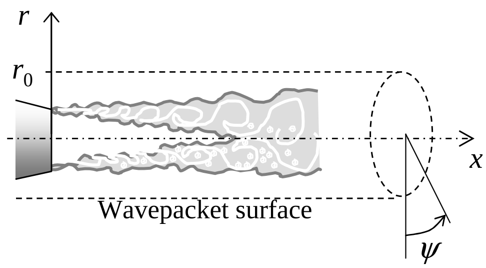

Figure 4. Wavepacket surface for the jet noise source.

B. Solution for Static Medium

1. *Exact solution*

Although we could use the general Kirchhoff formula to obtain the solution off the surface, it is more insightful to use the solution of the wave equation in cylindrical coordinates:

$$p(x,r,\psi) \;=\; \frac{1}{2\pi}e^{in\psi}\int_{-\infty}^{\infty}\widehat{p}_0(k_x)\frac{H_n^{(1)}(k_r r)}{H_n^{(1)}(k_r r_0)}e^{ik_x x}dk_x \tag{38}$$

$$\phi(x,r,\psi) \;=\; \frac{1}{2\pi}e^{in\psi}\int_{-\infty}^{\infty}\widehat{\phi}_0(k_x)\frac{H_n^{(1)}(k_r r)}{H_n^{(1)}(k_r r_0)}e^{ik_x x}dk_x \tag{39}$$

where

$$k_r \;=\; (k_x^2 - k^2)^{1/2}, \quad -\frac{\pi}{2} < \arg(k_r) < \frac{\pi}{2} \tag{40}$$

In Eqs. 38-40, $k = \omega/a_\infty$ is the acoustic wavenumber; $\hat{()}$ denotes the spatial Fourier transform; k_x is the axial wavenumber; k_r is the radial wavenumber; and $H_n^{(1)}$ is the Hankel function of the first kind of order n. The solution is radiating for $|k_x| \leq k$, for which k_r is real; and decaying for $|k_x| \geq k$, for which k_r is imaginary.

It is typical to prescribe an axial disturbance of the form $p_0(x) = A(x)e^{i\alpha x}$, with $A(x)$ the amplitude modulation and α the wavenumber of the instability. In that case, $\widehat{p}_0$ has the generic form

$$\widehat{p}_0(k_x) \;=\; \widehat{A}(k_x - \alpha) \tag{41}$$

This means that the Fourier transform is "centered" at the axial wavenumber $k_x = \alpha$. Figure 7 shows a symbolic graph of $\widehat{A}$ versus k_x. The instability wavenumber α is related to the convective Mach number M_c via

$$M_c \;=\; \frac{U_c}{a_\infty} \;=\; \frac{\omega/\alpha}{a_\infty} \;=\; \frac{k}{\alpha} \tag{42}$$

or

$$k \;=\; M_c\alpha \tag{43}$$

The example in Fig. 5 considers a subsonic instability with $M_c < 1$, therefore $k < \alpha$. Only the part of $\widehat{A}$ in the range $-k \leq k_x \leq k$ radiates to the far field. With increasing M_c more of the "energy" contained in $\widehat{A}$ radiates to the far field.

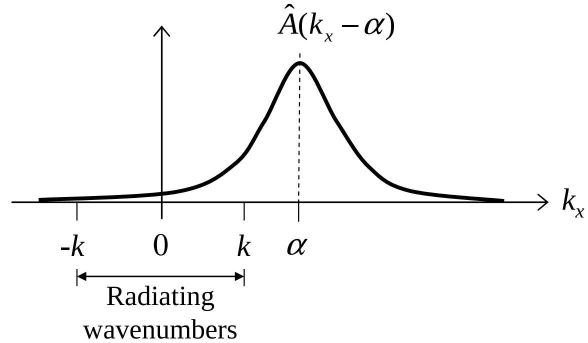

Figure 5. Wavepacket radiation for static case.

Recalling that p and ϕ are related through $p = ik\rho_\infty a_\infty \phi$, the corresponding relation of their transforms is

$$\widehat{p} = ik\rho_\infty a_\infty \hat{\phi} \tag{44}$$

2. Far-field approximation

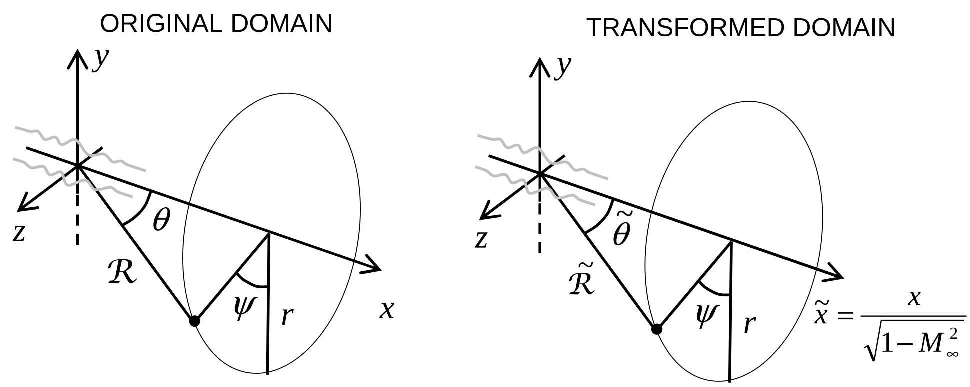

Figure 6. Coordinate system for far-field treatment of wavepacket.

Referring to the coordinate system of Fig. 6, when the observer is in the far field, Eq. 38 simplifies to

$$p(\mathcal{R}, \theta, \psi) = -\frac{i}{\pi \mathcal{R}} \frac{\widehat{p}_0(k\cos\theta)}{H_n^{(1)}(kr_0 \sin\theta)} e^{i(k\mathcal{R}+n\psi)} \tag{45}$$

The argument of $\widehat{p}_0$ ranges from $-k$ at $\theta = 180°$ to k at $\theta = 0°$, consistent with the range of radiating axial wavenumbers. The intensity in the far field is

$$|p|^2(\mathcal{R}, \theta) = \frac{1}{(\pi\mathcal{R})^2} \left| \frac{\widehat{p}_0(k\cos\theta)}{H_n^{(1)}(kr_0 \sin\theta)} \right|^2 \tag{46}$$

C. Solution for Subsonic Uniform Flow

The problem of a wavepacket in a uniform flow with Mach number $M_\infty < 1$ is now considered. Using the transformations listed in Eq. 17, the governing equation reduces to the ordinary Helmholtz equation. This means that the solutions for the static case, Eqs. 38-40, are valid in the transformed domain. Figure 7

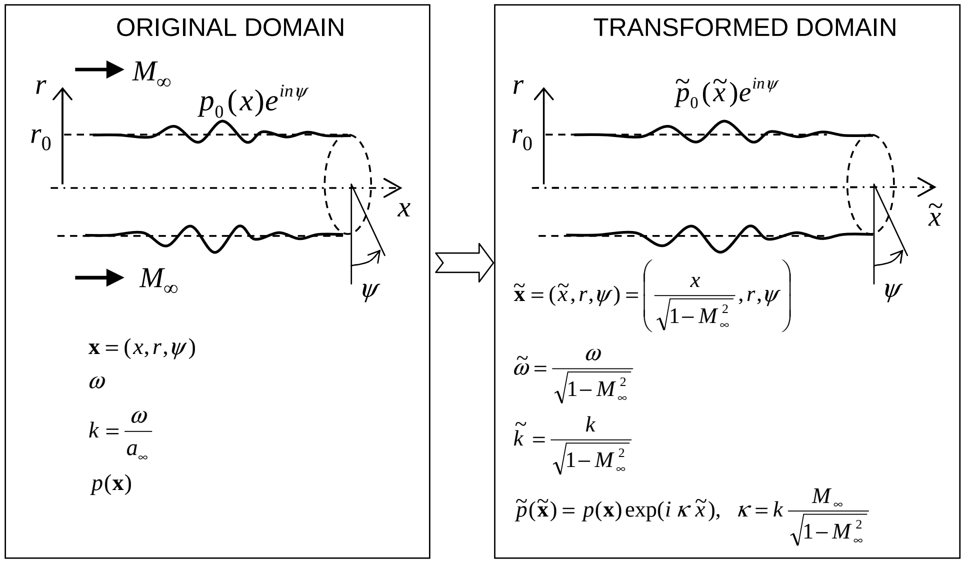

Figure 7. Transformation to static problem.

summarizes the variables and their transformations. The analysis that follows is done for the pressure but it is equally valid for the acoustic potential. The transformed pressure is

$$\widetilde{p} \;=\; p(\mathbf{x})e^{i\kappa\widetilde{x}}, \quad \kappa \;=\; k\frac{M_\infty}{\sqrt{1-M_\infty^2}} \tag{47}$$

It can be easily derived that the Fourier transform of $\widetilde{p}$ in $\widetilde{x}$ is

$$\widehat{\widetilde{p}}\,(k_{\widetilde{x}}, r, \psi) \;=\; \frac{1}{\sqrt{1-M_\infty^2}}\widehat{p}\left(\frac{k_{\widetilde{x}}-\kappa}{\sqrt{1-M_\infty^2}}, r, \psi\right) \tag{48}$$

1. *Exact solution*

The solution for $\widetilde{p}(\widetilde{\mathbf{x}})$ is obtained by using Eq. 38 in the transformed domain:

$$\widetilde{p}(\widetilde{x}, r, \psi) \;=\; \frac{1}{2\pi}e^{in\psi}\int_{-\infty}^{\infty}\widehat{\widetilde{p}}_0(k_{\widetilde{x}})\frac{H_n^{(1)}(k_r r)}{H_n^{(1)}(k_r r_0)}\exp(ik_{\widetilde{x}}\widetilde{x})dk_{\widetilde{x}} \tag{49}$$

with

$$k_r \;=\; (\widetilde{k}^2 - k_{\widetilde{x}}^2)^{1/2}, \quad -\frac{\pi}{2} < \arg(k_r) < \frac{\pi}{2} \tag{50}$$

Using Eq. 48,

$$\widetilde{p}(\widetilde{x}, r, \psi) \;=\; \frac{1}{2\pi}e^{in\psi}\frac{1}{\sqrt{1-M_\infty^2}}\int_{-\infty}^{\infty}\widehat{p}_0\left(\frac{k_{\widetilde{x}}-\kappa}{\sqrt{1-M_\infty^2}}\right)\frac{H_n^{(1)}(k_r r)}{H_n^{(1)}(k_r r_0)}\exp(ik_{\widetilde{x}}\widetilde{x})dk_{\widetilde{x}} \tag{51}$$

The inverse transformation $p(x, r, \psi) = \widetilde{p}(\widetilde{x}, r, \psi)\exp(-i\kappa\widetilde{x})$ gives the pressure in the original domain:

$$p(x, r, \psi) \;=\; \frac{1}{2\pi}e^{in\psi}\frac{e^{-i\kappa\widetilde{x}}}{\sqrt{1-M_\infty^2}}\int_{-\infty}^{\infty}\widehat{p}_0\left(\frac{k_{\widetilde{x}}-\kappa}{\sqrt{1-M_\infty^2}}\right)\frac{H_n^{(1)}(k_r r)}{H_n^{(1)}(k_r r_0)}\exp(ik_{\widetilde{x}}\widetilde{x})dk_{\widetilde{x}} \tag{52}$$

Letting k_x denote the argument $\widehat{p}_0$ in Eq. 52, and expressing all the coefficients in terms of k_x, the equation reduces to

$$p(x, r, \psi) \;=\; \frac{1}{2\pi}e^{in\psi}\int_{-\infty}^{\infty}\widehat{p}_0(k_x)\frac{H_n^{(1)}(k_r r)}{H_n^{(1)}(k_r r_0)}\exp(ik_x x)d\eta \tag{53}$$

with

$$k_r = \left[(k-k_xM)^2 - k_x^2\right]^{1/2}, \quad -\frac{\pi}{2} < \arg(k_r) < \frac{\pi}{2} \tag{54}$$

We recover the form of the static case, Eq. 38, except that the radial wavenumber contains Mach number effects. The roots of $k_r = 0$ are

$$k_x \;=\; -\frac{k}{1-M_\infty}\;,\quad \frac{k}{1+M_\infty}$$

Within the two roots, the pressure field is radiating. Outside the roots, the field is decaying. As M_∞ increases, the radiating band of axial wavenumbers shifts to the left, thus less energy is emitted to the far field. This trend is illustrated in Fig. 8.

2. Far field approximation

We apply the transformations of Eq. 17 to the far-field solution of Eq. 45. In the far-field coordinate system of Fig. 6, the stretching of the x-axis causes changes in the distance and polar angle of the observer. Denoting those variables $\widetilde{\mathcal{R}}$ and $\widetilde{\theta}$, respectively, the far-field solution is

$$\widetilde{p}(\widetilde{\mathcal{R}},\widetilde{\theta},\psi) \;=\; -\frac{i}{\pi\widetilde{\mathcal{R}}\sqrt{1-M_\infty^2}}\,\frac{\widehat{\widetilde{p}}_0(\widetilde{k}\cos\widetilde{\theta})}{H_n^{(1)}(\widetilde{k}r_0\sin\widetilde{\theta})}e^{i(\widetilde{k}\widetilde{\mathcal{R}}+n\psi)} \tag{55}$$

Using Eq. 48 and applying the inverse variable transformation, the pressure in the original domain is

$$p(\mathcal{R},\theta,\psi) \;=\; -\frac{i}{\pi\widetilde{\mathcal{R}}}\,\frac{e^{-i\kappa x}}{\sqrt{1-M_\infty^2}}\,\frac{\widehat{p}_0\left(\frac{\widetilde{k}\cos\widetilde{\theta}-\kappa}{\sqrt{1-M_\infty^2}}\right)}{H_n^{(1)}(\widetilde{k}r_0\sin\widetilde{\theta})}e^{i(\widetilde{k}\widetilde{\mathcal{R}}+n\psi)} \tag{56}$$

It is convenient to express the transformed distances in terms of the parameters R and R^* defined for the Green's function, Eq. 21, tailored to the coordinate system of Fig. 6:

$$\begin{aligned}
p(\mathcal{R},\theta,\psi) \;&=\; -\frac{i}{\pi R^*}\,\frac{\widehat{p}_0\left(\frac{k(\cos\widetilde{\theta}-M_\infty)}{1-M_\infty^2}\right)}{H_n^{(1)}\left(\frac{k}{\sqrt{1-M_\infty^2}}r_0\sin\widetilde{\theta}\right)}e^{i(kR+n\psi)} \\
R \;&=\; \frac{1}{1-M_\infty^2}\left[R^* - M_\infty x\right] \\
R^* \;&=\; \sqrt{x^2+(1-M_\infty^2)r^2}
\end{aligned} \tag{57}$$

Equation 58 shows explicitly the effect of Mach number M_∞ on the far-field radiation of the wavepacket. As $\widetilde{\theta}$ increases from 0 to π, the argument of $\widehat{p}_0$ ranges from $k/(1+M_\infty)$ to $-k/(1-M_\infty)$. This is consistent with the behavior of the exact solution discussed previously and illustrated in Fig. 8.

Finally, the far-field intensity is

$$|p|^2(\mathcal{R},\theta) \;=\; \frac{1}{(\pi R^*)^2}\left|\frac{\widehat{p}_0\left(\frac{k(\cos\widetilde{\theta}-M_\infty)}{1-M_\infty^2}\right)}{H_n^{(1)}\left(\frac{k}{\sqrt{1-M_\infty^2}}r_0\sin\widetilde{\theta}\right)}\right|^2 \tag{58}$$

with R^* defined in Eq. 58. In Eqs. 56-58, the transformed polar angle is obtained from

$$\widetilde{\theta} \;=\arctan\left(\sqrt{1-M_\infty^2}\;\tan\theta\right) \tag{59}$$

3. Examples

The examples that follow simulate the source of a jet with velocity U_j=400 m/s, radius r_0, and Strouhal number $Sr = 2fr_0/U_j = 0.2$. The convective velocity of the instability wave is assumed to be $U_c =$

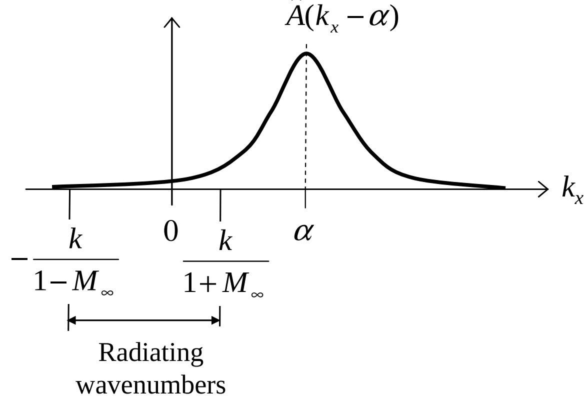

Figure 8. Wavepacket radiation for uniform subsonic flow.

$0.7U_j = 280$ m/s. The speed of sound is $a_\infty = 345$ m/s, thus the convective Mach number is subsonic at $M_c = U_c/a_\infty$=0.81. We consider a Gaussian wavepacket with pressure distribution on $r = r_0$ prescribed as

$$p_0(x) \;=\; e^{-[(x-b)/b]^2} e^{iax}$$

with $b = 4r_0$ and the instability wavenumber satisfying $\alpha = \omega/U_c$. The exact solution of the pressure field, Eq. 53, is computed for Mach numbers M_∞=0.00, 0.20, 0.50, and 0.81. The significance of the last Mach number is that it equals the convective Mach number of the instability, thus the "relative" Mach number of the instability is zero.

Figure 9 plots isocontours of the the real part and the magnitude of the pressure field for the different free-stream Mach numbers. With increasing Mach number the pressure field weakens considerably. However, even at $M_\infty = 0.81$ (where the relative Mach number of the instability is zero) there is a finite amount of energy being radiated to the far field. This is evident from the radiating wavenumber band of Fig. 8: M_∞ may increase up to 1.0 (the limit of this analysis) and there is still some wavepacket energy in the range $k_x = -\infty$ to $k/2$. The far-field intensity is computed using Eq. 59. Figure 10 plots the intensity at fixed radius versus polar angle for the aforementioned free-stream Mach numbers. The intensity levels decline, particularly at the high polar angles. This produces a narrowly focused beam of acoustic energy at low polar angles for this particular wavepacket form.

V. Source Parameterization

A. General Concept

The noise source model can be expressed in terms of a finite set of parameters, which are determined from acoustic field measurements. This process is called parameterization. The field $\mathbf{F}$ is typically represented in the form of statistics such as auto-spectra or cross-spectra. Denote $\mathbf{F} = F_1, F_2, \ldots F_N$ denote the field at points $n = 1, 2, \ldots, N$. The modeled field is cast in terms of a parameter vector A_j, $j = 1, \ldots, J$:

$$\mathbf{F}_{\mathrm{mod}}(A_j)$$

The experimental field is $\mathbf{F}_{\mathrm{exp}}$. The parameter vector is sought via the least-squares minimization of

$$f(A_j) \;=\; ||\mathbf{F}_{\mathrm{mod}}(A_j) - \mathbf{F}_{\mathrm{exp}}||^2 \tag{60}$$

Various minimization approaches are available for this task, including the conjugate-gradient method.

B. Parameterization Based on Autospectra

Perhaps the simplest type of parameterization involves "matching" of the modeled and experimental autospectra (intensities) in the far field. In the past, the incoherent combination of a wavepacket and a monopole was used to simulate the acoustic intensity in the far field of a jet. These simulations were done

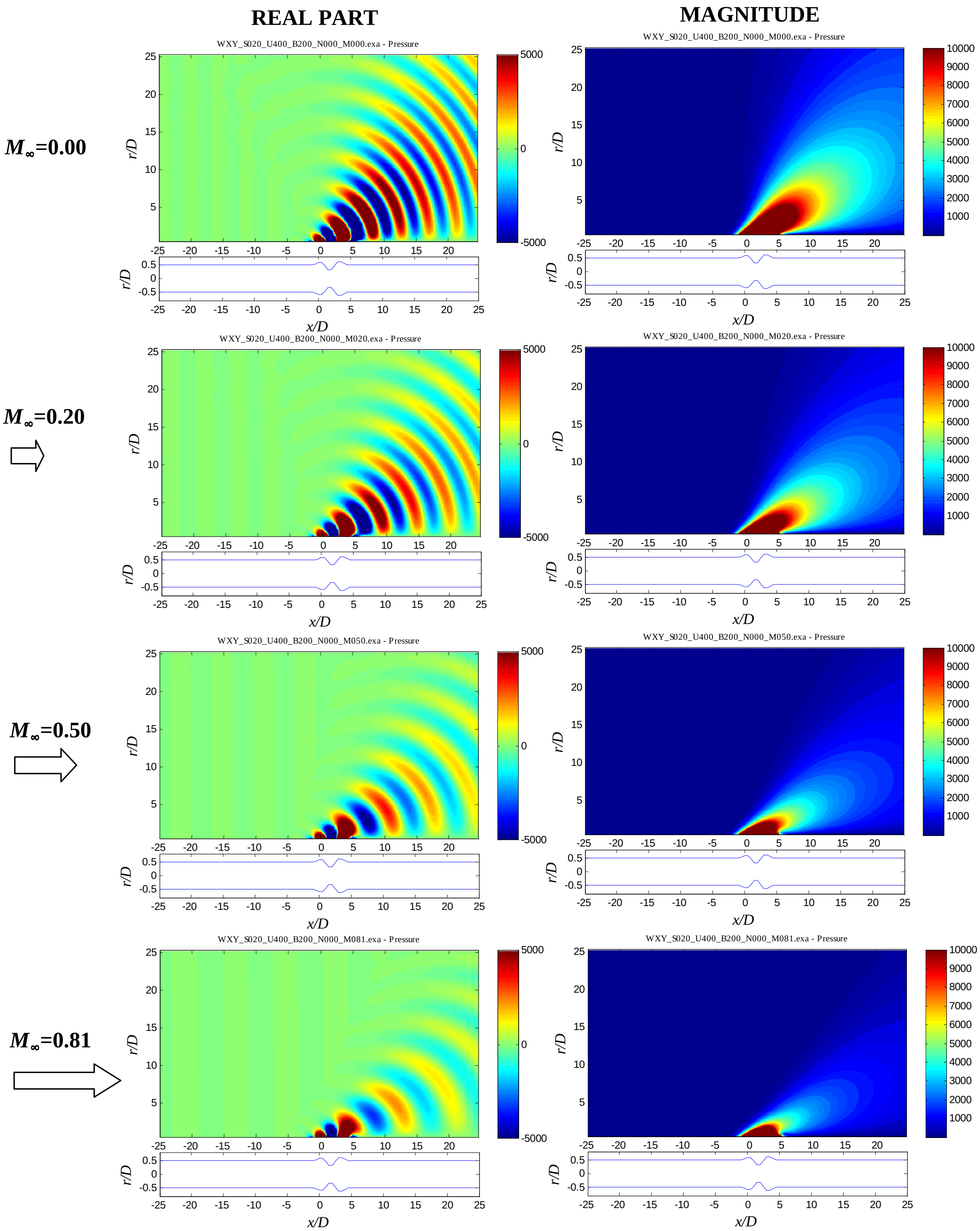

Figure 9. Pressure field of Gaussian wavepacket with increasing Mach number.

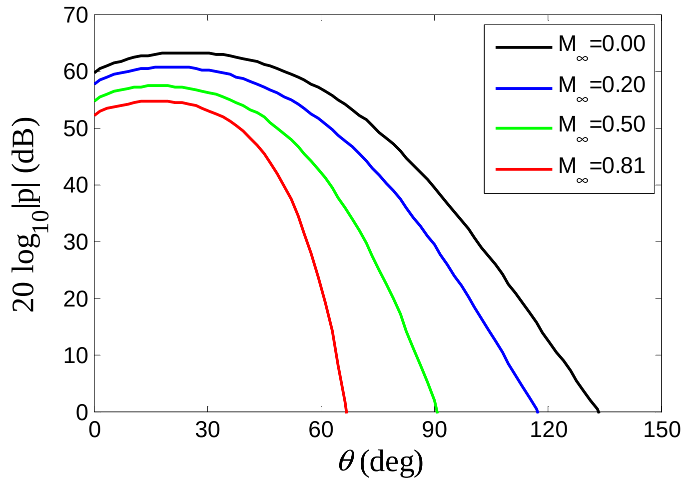

Figure 10. Polar directivity of far-field intensity for Gaussian wavepacket.

at static conditions. This section presents the corresponding relations for parameterizing the noise source with forward flight. The modeled far-field intensity for a given frequency is

$$|p|^2_{mod} \;=\; |p|^2_w \;+\; |p|^2_m \tag{61}$$

where the subscripts w and m refer to the wavepacket and the monopole, respectively. Using Eqs. 58 and 34,

$$|p|^2_{mod}(\mathbf{x}, A_j) = \frac{1}{(\pi R^*)^2}\left\{\left|\frac{\widehat{p}_0\left(\frac{k(\cos\widetilde{\theta}-M_\infty)}{1-M_\infty^2}, A_{1,\ldots,J-1}\right)}{H_n^{(1)}\left(\frac{k}{\sqrt{1-M_\infty^2}}r_0\sin\widetilde{\theta}\right)}\right|^2 + A_J^2\left(\frac{\rho_\infty a_\infty k}{4}\;\frac{1-M_\infty\frac{x}{R^*}}{1-M_\infty^2}\right)^2\right\} \tag{62}$$

Here the wavepacket shape $p_0(x)$ is parameterized in terms of A_j, $j=1,\ldots,J-1$; and the monopole strength is A_J. As before, the transformed distance R^* is

$$R^* = \sqrt{x^2+(1-M_\infty^2)r^2}$$

Alternatively the monopole can be replaced by the fictitious pressure point source (PPS) discussed in Section IV.B:

$$|p|^2_{mod} \;=\; |p|^2_w \;+\; |p|^2_{\mathrm{PPS}} \tag{63}$$

Then

$$|p|^2_{mod}(\mathbf{x}, A_j) = \frac{1}{(\pi R^*)^2}\left\{\left|\frac{\widehat{p}_0\left(\frac{k(\cos\widetilde{\theta}-M_\infty)}{1-M_\infty^2}, A_{1,\ldots,J-1}\right)}{H_n^{(1)}\left(\frac{k}{\sqrt{1-M_\infty^2}}r_0\sin\widetilde{\theta}\right)}\right|^2 + \frac{A_J^2}{16}\right\} \tag{64}$$

with A_J now representing the strength of the PPS.

VI. Boundary Element Method with Uniform Flow

Having established the propagation relations of monopole and wavepacket sources in a uniform subsonic freestream, we provide guidelines on their implementation in computational problems using the BEM reviewed in Section II.B. The BEM is a powerful method for solving radiation and scattering problems. Available implementations of the BEM solve the canonical Helmholtz equation. For acoustic problems with uniform flow, the BEM must be used in the transformed domain. In the study of propulsion/airframe integration effects, the BEM can be used for computing both the scattered field and the radiated field of complex surface-prescribed sources like the wavepacket. The analytical solution of wavepacket emission (e.g., Eq. 38) requires the use of a Fast Fourier Transform (FFT) at each surface and field point, a process that is computationally demanding and can require a long time before the incident field is computed. The BEM can give a faster solution, particularly when a large number of field points is involved.

If the problem involves a scattering surface, this surface must be slender to justify the uniform flow approximation. In other words, the slopes must be very small. Under this condition, the solid boundary condition in the transformed domain is approximately the same as in the original domain:

$$\begin{aligned} \frac{\partial \widetilde{p}}{\partial \widetilde{n}} &\approx 0 \\ \frac{\partial \widetilde{\phi}}{\partial \widetilde{n}} &\approx 0 \end{aligned} \tag{65}$$

The sections that follow detail the BEM implementation for the wavepacket, monopole, and pressure point source. In all cases, the source parameters would be determined through the parameterization scheme discussed in Section V.

A. Wavepacket

The computation process for the wavepacket is summarized in Fig. 11. Having done the parameterization approach of Section V, the wavepacket surface pressure distribution on $r = r_0$, $p_0(x)e^{in\psi}$, is known in the original domain.

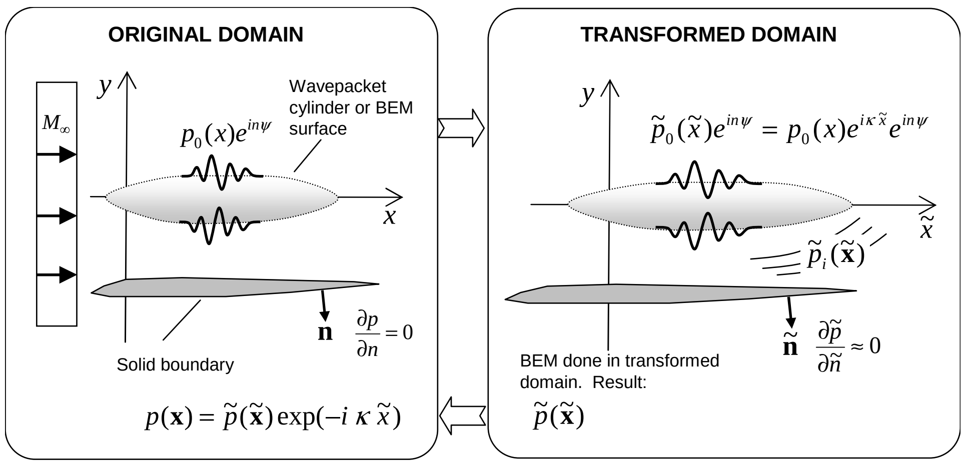

Figure 11. BEM approach for wavepacket.

Moving now to the transformed domain, using the variable transformation of Eq. 47, the prescribed pressure on the wavepacket surface is

$$\widetilde{p}_0(\widetilde{x}) \;=\; p_0(x)e^{i\kappa\widetilde{x}}$$

The problem now involves the transformed frequency $\widetilde{\omega} = \omega/\sqrt{1 - M_\infty^2}$ (cyclic frequency $\widetilde{f} = f/\sqrt{1 - M_\infty^2}$) and transformed acoustic wavenumber $\widetilde{k} = \widetilde{\omega}/a_\infty$. The exact solution for the pressure field is given by Eq. 49. In essence, we are solving the static problem with a different surface pressure distribution and a different acoustic wavenumber. The resulting pressure field is the incident field $\widetilde{p}_i(\widetilde{\mathbf{x}})$ for scattering problems. To clarify how the transformed surface pressure differs from the one in the original domain, suppose that $p_0(x)$ has the form

$$p_0(x) = A\left(\frac{x}{L}\right)\exp(i\alpha x)$$

with α the instability wavenumber and L a characteristic length scale of the amplitude modulation. In the transformed domain, we have

$$\widetilde{p}_0(\widetilde{x}) \;= A\left(\frac{\widetilde{x}}{L/\sqrt{1 - M_\infty^2}}\right)\exp\left[i(\alpha\sqrt{1 - M_\infty^2} + \kappa)\widetilde{x}\right]$$

The first-order effect is the addition of κ to the spatial oscillation frequency which increases the wavenumber of the instability in the transformed domain. The second-order effect, from the $\sqrt{1 - M_\infty^2}$ terms, is the stretching of the amplification envelope; it is a minor effect unless M_∞ is high subsonic. Figure 14 demonstrates these effects by assuming $A(x/L) = \exp[-(x/L)^2]$, $L = 1$, $\alpha = 1$, and $k = 0.8$. The transformation for Mach numbers 0.3 and 0.8 is shown. For $M_\infty = 0.3$, we note the increased spatial frequency with minor stretching of the envelope. At $M_\infty = 0.8$, the spatial oscillation becomes rapid and the envelope is elongated significantly.

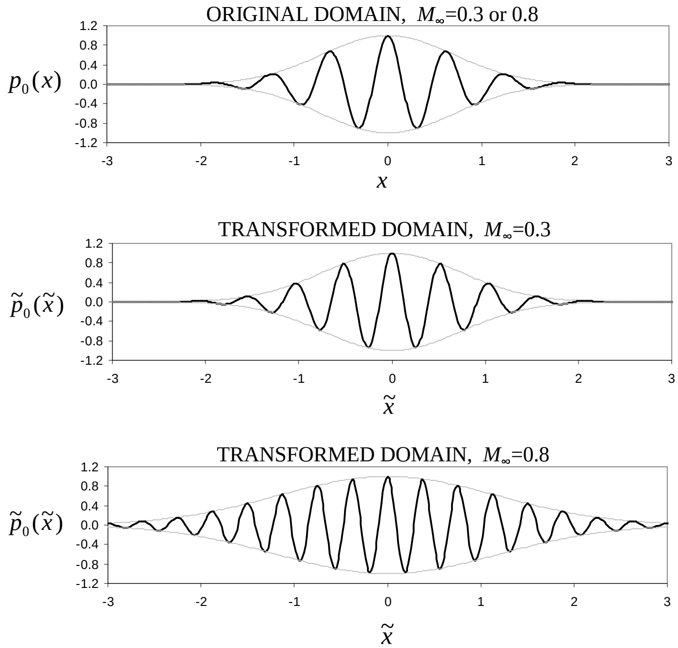

Figure 12. Illustration of how the waveform $p_0(x)$ changes in the transformed domain for $M_\infty = 0.3$ and 0.8.

The scattering surface is represented in the $\widetilde{\mathbf{x}}$ domain by stretching its $x-$ coordinates by the factor $1/\sqrt{1-M_\infty^2}$. With the wavepacket incident field computed, the BEM gives the total (scattered plus incident) field $\widetilde{p}(\widetilde{x})$ in the transformed domain. The pressure field in the original domain is obtained from the inverse transformation

$$p(\mathbf{x}) \;=\; \widetilde{p}(\widetilde{\mathbf{x}})e^{-i\kappa\widetilde{x}}$$

B. Monopole

The treatment of the monopole warrants particular attention because of the complexities discussed in Section III.B. Referring to Fig. 13, the strength of the monopole Q is determined through the parameterization process of Section V (Eq. 63). This strength is then used to compute the *acoustic potential* field in the transformed domain using the static version of Eq. 29:

$$\widetilde{\phi}(\widetilde{\mathbf{x}}) \;=\; \frac{Q}{4\pi|\widetilde{\mathbf{x}}-\widetilde{\mathbf{x}}_s|}e^{i\widetilde{k}|\widetilde{\mathbf{x}}-\widetilde{\mathbf{x}}_s|}$$

where $\widetilde{\mathbf{x}}_s$ is the center of the monopole in the transformed domain. In scattering problems, this is the incident field $\widetilde{\phi}_i(\widetilde{\mathbf{x}})$. The BEM then gives the total field $\widetilde{\phi}(\widetilde{\mathbf{x}})$ in the transformed domain. The inverse variable transformation gives the acoustic-potential field in the original domain:

$$\phi(\mathbf{x}) \;=\; \widetilde{\phi}(\widetilde{\mathbf{x}})e^{-i\kappa\widetilde{x}}$$

and the pressure is obtained from Eq. 14.

C. Pressure Point Source (PPS)

Referring to Fig. 14, the strength Q of the PPS is determined from the parameterization process of Section V (Eq. 65). The strength is then used to compute the pressure in the transformed domain using the Green's

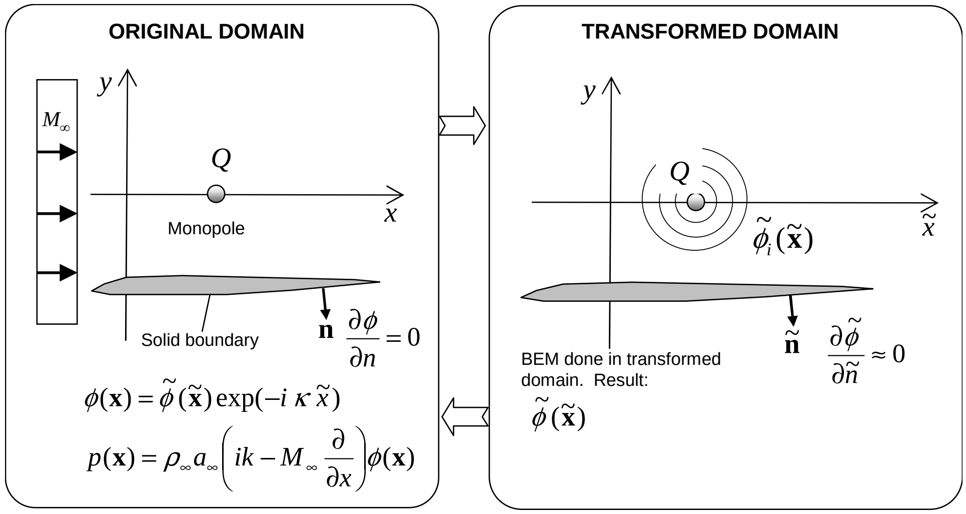

Figure 13. BEM approach for monopole.

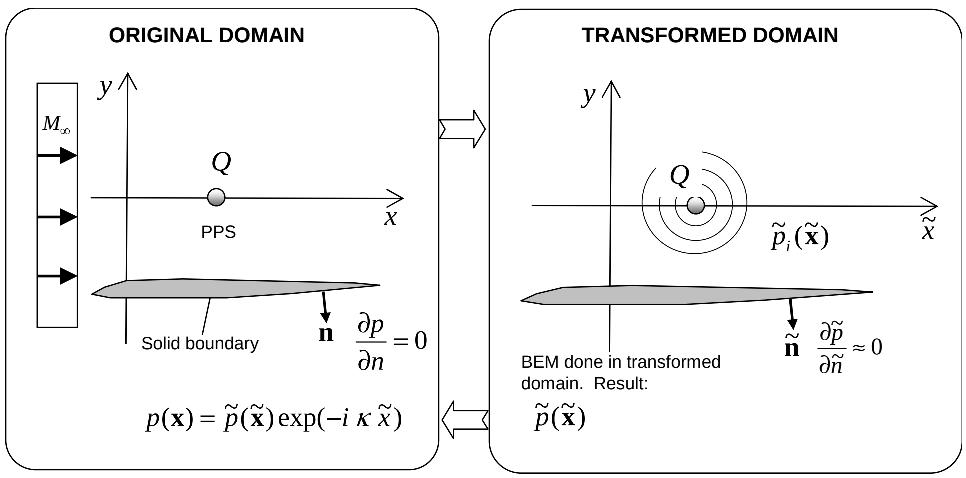

Figure 14. BEM approach for pressure point source (PPS).

function, Eq. 19:

$$\widetilde{p}(\widetilde{\mathbf{x}}) \;=\; \frac{Q}{4\pi|\widetilde{\mathbf{x}}-\widetilde{\mathbf{x}}_s|}e^{i\widetilde{k}|\widetilde{\mathbf{x}}-\widetilde{\mathbf{x}}_s|}$$

where $\widetilde{\mathbf{x}}_s$ is the center of the PPS in the transformed domain. In scattering problems, this is the incident field $\widetilde{p}_i(\widetilde{\mathbf{x}})$. Using the BEM one obtains the total field $\widetilde{p}(\widetilde{\mathbf{x}})$ in the transformed domain. The inverse variable transformation gives the pressure field in the original domain:

$$p(\mathbf{x}) \;=\; \widetilde{p}(\widetilde{\mathbf{x}})e^{-i\kappa\widetilde{x}}$$

D. BEM Surface for Wavepacket

As an alternative to the analytical solution of the wavepacket incident field, which can be computationally demanding, the BEM may be used to compute the radiated field of the wavepacket. The computational mesh for this purpose is illustrated in Fig. 15. The source length $X_{source}$is based on the criterion of the envelope amplitude exceeding a certain threshold, typically 10^{-4} times the peak value. To minimize end effects, it is recommended that the mesh be three times as long, adding one source length upstream and one downstream of the source region. The grid resolution Δ is based on the typical BEM criterion $\Delta \leq \lambda/8$. For low frequencies, the wavelength may be too large for this criterion to resolve the cigar-shaped mesh. In that case, a perimeter-based criterion should be used, e.g., $\Delta \leq 2\pi r_0/10$. In summary, a rough rule of thumb is

$$\Delta = \min\left(\frac{\lambda}{8}, \frac{\pi r_0}{5}\right)$$

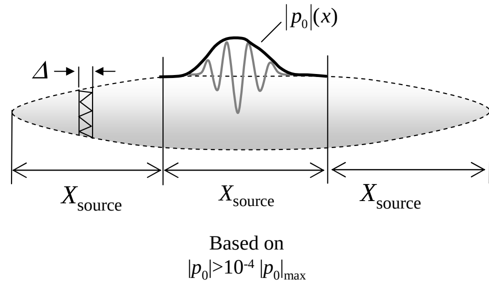

Figure 15. Wavepacket BEM surface.

E. Examples

We offer a few examples of scattering using the wavepacket model at static conditions and in forward flight. The fast-multipole version of BEM was used, as implemented in the FastBEM software package (Advanced CAE Research, LLC; see also Ref. 14). The examples that follow demonstrate the methodology developed in this paper and do not seek to represent any realistic configurations. It should be noted that the same wavepacket model is used at static and forward-flight conditions. This is not realistic as the wavepacket parameters will change based on the parameterizations at these two conditions. The scarcity of available and reliable jet noise data with forward flight, with sufficiently resolved polar directivity of the sound pressure level spectrum, has not allowed rigorous implementation of the parameterization scheme of Section V with forward flight.

The jet simulation is based on the recent work of Papamoschou.[1] We consider a single-stream subsonic jet with $M_j = 0.9$, $U_j = 280$ m/s, and $D_j = 0.022$ m. The Strouhal number is $Sr = fD_j/U_j = 0.5$ The pressure on the wavepacket surface $r = r_0$ is

$$p_0(x, \psi) = \tanh(x/b_1)^{p_1} \; [1 - \tanh(x/b_2)^{p_2}] \, e^{i\alpha x} e^{in\psi}$$

with $\alpha = 276$ m^{-1} (corresponding to $U_c/U_j = 0.52$), $b_1/D_j = 1.45$, $b_2/D_j = 2.60$, $p_1 = 1.84$, $p_2 = 2.84$, and $n = 2$. These values reflect the parameterization based on far-field autospectra at static conditions.[1] The scattering surface is a rectangular plate with span of 0.5 m, chord of 0.2 m, and thickness of 0.02 m. The shield is located 0.05 m below the jet centerline. The peak of the radiating part of $p_0(x)$ is located 0.046 m upstream of the trailing edge.

Figure 16 shows contour plots of the incident and total pressure fields for $Sr = 0.5$ at $M_\infty = 0.0$ and 0.50. The weakening of the incident field with forward flight is evident. For this particular wavepacket the direction of peak emission at $M_\infty = 0.50$ shifts to higher angle. Together with the overall compaction of the radiating noise source, this increases the effectiveness of the shielding as seen in the contours of the total pressure. The benefit of the forward flight effect on shielding is further evident in the plots of Fig. 17 which show the polar directivity of the intensities of the incident and total pressure fields. Note that these results are normalized so that the peak of the unshielded distribution is set at 0 dB. In the downward direction, increasing the flight Mach number from 0 to 0.5 increases the effectiveness of the shield (in terms of reducing the peak amplitude) from 3 dB to 12 dB. In the sideline direction, the corresponding attenuation increases from 1 dB to 5 dB.

The results of Figs. 16 and 17 indicate that, for the same wavepacket source, the mean flow is expected to have a beneficial effect on shielding. Not factored in these predictions is the physical change of the noise source with increasing forward velocity. For a jet issuing from a regular nozzle, the noise source region will elongate with increasing Mach number, thus counteracting the source compaction trend. The elongation of the noise source region could possibly be inferred from the parameterization scheme of Section V, however

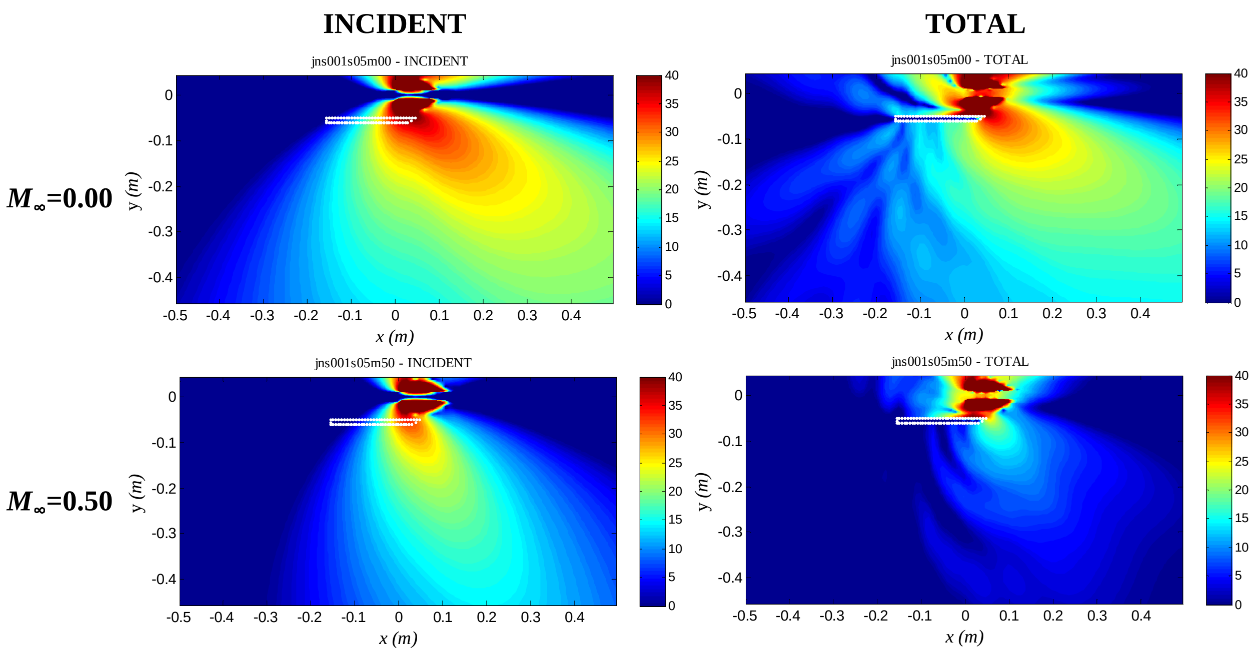

Figure 16. Intensities on symmetry plane of incident and total pressure fields (dB) for wavepacket diffraction of from a rectangular-plate shield at Strouhal number $Sr = 0.5$. Shield cross section is indicated by the while dots.

this hypothesis was not tested due to the aforementioned lack of experimental data. On the other hand, a jet issuing from a nozzle with aggressive mixing devices, such as deep-penetrating chevrons, may not experience significant elongation of the noise source region with forward flight. For practical aircraft configurations, aggressive nozzle devices are essential for achieving significant jet noise shielding.[15]

VII. Conclusion

The paper presented a methodology for treating the emission and diffraction of elementary jet noise sources in the presence of a uniform subsonic mean flow. The analysis included wavepacket and point sources. The governing equations were reduced to the canonical wave equation through established transformations in the dependent variable and the axial coordinate. The impact of the transformations on the emission of the isolated sources was elucidated, with attention on the distinction between sources of pressure and sources of volume.

For a monopole source, the uniform flow significantly complicates the pressure field with different near- and far-field scaling laws and with upstream amplification. The impact of the transformations on the wavepacket emission is two-fold: shifting of the range of radiating wavenumbers and, for large Mach numbers, elongation of the wavepacket envelope in the transformed domain. Both effects reduce the radiation efficiency of the wavepacket source and compact the extent of the radiating noise source region.

The boundary element method was applied in the transformed domain to compute the scattered field from a solid object, in this case a thin flat plate. The pressure field in the physical domain was obtained by reversing the transformations. Because of the aforementioned compaction of the noise source, the effectiveness of the shielding increased with increasing Mach number of the uniform flow.

Acknowledgement

We gratefully acknowledge the support by NASA Contract NNL08AA00B, monitored by Dr. Casey Burley.

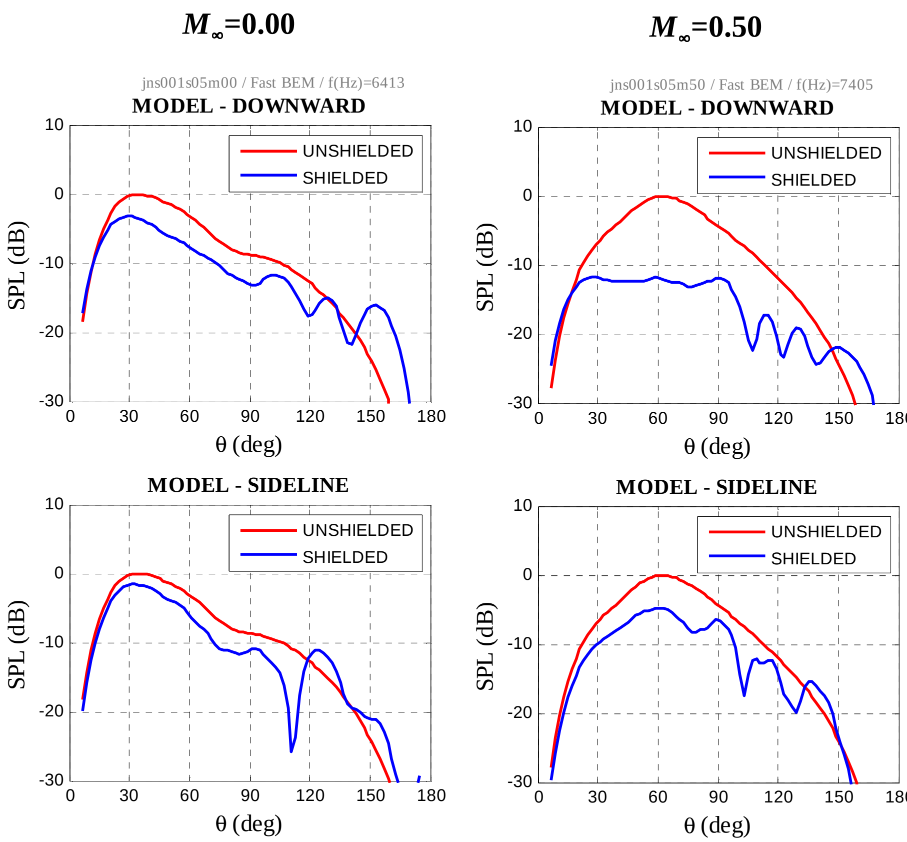

Figure 17. Polar directivity of far-field intensity for the configurations of Fig. 16. The downward and sideline data correspond to $\psi = 0°$ and $\psi = 60°$, respectively.

References

[1]Papamoschou, D., "Prediction of Jet Noise Shielding," AIAA 2010-0653, Jan. 2010.

[2]Wu, T., *Boundary Element Acoustics*, WIT Press, Boston, 2000.

[3]Tinetti, A. and Dunn, M., "Aeroacoustic Noise Prediction Using the Fast Scattering Code," AIAA 2005-3061, May 2005.

[4]Taylor, K., "A Transformation of the Acoustic Equation with Implications for Wind-Tunnel and Low- Speed Flight Tests," *Proceedings of the Royal Society of London*, Vol. 363, No. 1713, Nov. 1978, pp. 271–281.

[5]Blokhintsev, D., "Acoustics of a Nonhomogeneous Moving Medium," NACA TM-1399, 1956.

[6]Najafi-Yazdi, A., Bres, G., and Mongeau, L., "An Acoustic Analogy Formulation for Moving Source in Uniformly Moving Media," *Proceedings of the Royal Society A*, Vol. 467, No. 2125, Jan. 2010, pp. 144–165.

[7]Wu, T. and Lee, L., "A Direct Boundary Integral Formulation For Acoustic Radiation In A Subsonic Uniform Flow," *Journal of Sound and Vibration*, Vol. 175, Aug. 1994, pp. 51–63.

[8]Lyrintzis, A. and Mankbadi, R., "Prediction of the Far-Field Jet Noise Using Kirchhoff's Formulation," *AIAA Journal*, Vol. 34, Feb. 1996, pp. 413–416.

[9]Tam, C. and Burton, D., "Sound Generation by the Instability Waves of Supersonic Flows. Part 2. Axisymmetric Jets," *Journal of Fluid Mechanics*, Vol. 138, 1984, pp. 273–295.

[10]Crighton, D. and Huerre, P., "Shear-Layer Pressure Fluctuations and Superdirective Acoustic Sources," *Journal of Fluid Mechanics*, Vol. 220, 1990, pp. 355–368.

[11]Avital, E., Sandham, N., and Luo, K., "Mach Wave Radiation by Mixing Layers. Part I: Analysis of the Sound Field," *Theoretical and Computational Fluid Dynamics*, Vol. 12, 1998, pp. 73–90.

[12]Morris, P., "A Note on Noise Generation by Large Scale Turbulent Structures in Subsonic and Supersonic Jets," *International Journal of Aeroacoustics*, Vol. 8, No. 4, 2009, pp. 301–316.

[13]Reba, R., Narayanan, S., and Colonius, T., "Wave-Packet Models for Large-Scale Mixing Noise," *International Journal of Aeroacoustics*, Vol. 9, 2010, pp. 533–558.

[14]Liu, Y., *Fast Multipole Boundary Element Method - Theory and Applications in Engineering*, Cambridge University Press, Cambridge, 2009.

[15]Papamoschou, D. and Mayoral, S., "Jet Noise Shielding for Advanced Hybrid Wing-Body Configurations," AIAA 2011-912, Jan. 2011.